

# Study of the acid and redox properties of copper oxide supported on ceria–zirconia in isopropyl and *t*-butyl alcohol conversion

Monika Radlik<sup>1</sup> · Joanna Strzezik<sup>1</sup> ·  
Agnieszka Krowiak<sup>1</sup> · Krzysztof Koziel<sup>1</sup> ·  
Andrzej Krztoń<sup>2</sup> · Wincenty Turek<sup>1</sup>

Received: 8 January 2015 / Accepted: 29 March 2015 / Published online: 3 April 2015  
© Akadémiai Kiadó, Budapest, Hungary 2015

**Abstract** The CuO/Ce<sub>0.62</sub>Zr<sub>0.38</sub>O<sub>2</sub> catalysts with different Cu loading were prepared by incipient wetness impregnation. The amount of Cu was 2, 4, 10 wt%. The samples were characterized by X-ray diffraction, scanning electron microscopy (SEM/EDX), N<sub>2</sub> adsorption and Raman spectroscopy. The acid and redox properties of these catalysts were evaluated by isopropyl and *t*-butyl alcohol conversion. The isopropyl alcohol conversion showed that all Cu/CZ catalysts possessed higher activity than pure CuO and unmodified CZ support in dehydrogenation to acetone. The strong interaction of the active phase with the support is responsible for this rise of activity. Conversion of *t*-butyl alcohol confirmed the presence of acid centres. It was found that the increase in the activity of Cu/CZ catalysts compared with the unmodified CZ support is caused by the CuO active phase.

**Keywords** CuO/CeZrO<sub>2</sub> · Acid properties · Redox properties

## Introduction

More than 90 % of the industrial production of chemicals is based on catalytic processes. The most desired catalytic systems are those with multifunctional active sites enabling efficient conversion of the reactants into expected products.

**Electronic supplementary material** The online version of this article (doi:10.1007/s11144-015-0865-9) contains supplementary material, which is available to authorized users.

✉ Joanna Strzezik  
joanna.strzezik@polsl.pl

<sup>1</sup> Department of Physical Chemistry and Technology of Polymers, Silesian University of Technology, M. Strzody 9, 44-100 Gliwice, Poland

<sup>2</sup> Centre of Polymer and Carbon Materials, Polish Academy of Sciences, M. Curie-Skłodowskiej 34, 41-819 Zabrze, Poland

Bifunctional catalysts with both acid–base and redox properties have been successfully used in various industrial processes such as: reforming, partial oxidation of light hydrocarbons and deNO<sub>x</sub> reactions [1–5]. The crucial parameters influencing the catalytic activity of these systems are acid–base and redox properties of their active sites. Therefore, the evaluation of acid–base and redox surface properties of the catalysts has a key role in determination of the reaction mechanism and elaboration of new catalytic systems with most suitable parameters.

There are many different methods to determine the acid–base or redox properties of the catalysts. They can be characterized by spectroscopy, temperature programmed desorption of species like CO, NH<sub>3</sub> or test reactions [3, 6–8]. The most popular catalytic test reactions are conversion of alcohols (isopropanol, 2-butanol), isomerization of alkenes (1-butene) and cracking of hydrocarbons (neopentane, cumene) [9–12]. The two latter groups of test reactions are often applied in studies on acid–base catalysts while alcohol conversion is also used for examination of redox catalysts.

The conversion of isopropyl alcohol is the most common test reaction for the determination of both acid–base and redox properties of catalysts [8, 13–15]. The process, in general, consists of three parallel reactions i.e.: dehydration to propene, dehydrogenation to acetone and intermolecular dehydration to diisopropyl ether. Dehydration to propene runs over acid or acid–base active sites and can be used to examine their activity. Dehydrogenation to acetone gives information about activity of redox and base active sites, while intermolecular dehydration to diisopropyl ether tests the properties of acid active sites [8, 13–16].

The main product of *t*-butyl alcohol conversion is isobutene, formed as a result of dehydration of alcohol molecules. This reaction is an indicator of the activity of the catalyst acid sites.

In the past few years, ceria-zirconia mixed oxides have often been examined as the supports or catalysts in various catalytic processes. These oxides are among the most important components of catalytic systems in the NO<sub>x</sub> reduction process [17, 18]. The application of ceria-zirconia as the support is due to the oxygen storage/release capacity, high surface area and good stability [19, 20]. Moreover, ceria-zirconia has a promotional effect on noble and transition metals (or oxides) caused by the specific metal-support interaction, which improves stability, enables high dispersion and upgrades the redox properties of the active phase [21–24]. The promotional effect of ceria-zirconia on the catalytic properties is also observed for catalysts consisting of CuO dispersed on CeZrO<sub>2</sub> [25, 26]. The CuO/CeZrO<sub>2</sub> catalytic system, due to its high activity and low price, is an alternative for the noble metals (Rh, Pt) supported ceria-zirconia catalysts in the deNO<sub>x</sub> process [26]. The CuO/CeZrO<sub>2</sub> catalysts can be applied in the selective catalytic reduction of NO by hydrocarbons (HC-SCR) [26]. The literature data reveal that the HC-SCR reaction pathway strongly depends on the catalyst and type of hydrocarbon used as a reducing agent [27]. The reduction of NO and the activation of hydrocarbons proceed over redox and acid–base sites respectively [28]. Therefore, catalysts applied in HC-SCR should have both acid–base and redox active sites on their surface. In the literature, there are many studies concerning the redox properties of ceria-zirconia catalysts [17, 25, 26, 29]. Unfortunately, despite the role of acid–base

sites and their evolution at variable temperature in the HC-SCR catalytic process, very little data have been published about acid–base properties of CuO/CeZrO<sub>2</sub> catalysts.

In this work, a series of CuO/CeZrO<sub>2</sub> catalysts with different Cu loading was prepared.

The activity of examined catalysts was determined using the conversion of isopropyl and *t*-butyl alcohol. The influence of various amounts of Cu in CuO/CeZrO<sub>2</sub> on the catalytic activity and physicochemical properties of catalysts were established. A correlation between the results obtained from the test reactions and temperature programmed reduction was found.

## Experimental

C<sub>3</sub>H<sub>7</sub>OH (99.5 %), C<sub>4</sub>H<sub>9</sub>OH (99.5 %), Cu(NO<sub>3</sub>)<sub>2</sub>·3H<sub>2</sub>O were purchased from POCH, and Ce<sub>0.62</sub>Zr<sub>0.38</sub>O<sub>2</sub> was provided by RHODIA Electronics & Catalysts, CuO (98 %) was purchased from AnalaR. All reagents were analytical grade and were used as received.

### Catalyst preparation

A series of CuO/Ce<sub>0.62</sub>Zr<sub>0.38</sub>O<sub>2</sub> (named as Cu/CZ) catalysts with different amounts of copper was prepared by the incipient wetness impregnation of the commercial support. The CZ support was impregnated with copper(II) nitrate aqueous solution. In the next step, the samples were dried in the air at 393 K for 12 h and calcined at 823 K for 2 h. The amount of Cu was 2, 4, 10 wt% (Table 1) and the obtained catalysts were denoted as Cu(2)/CZ, Cu(4)/CZ and Cu(10)/CZ.

### Characterization of the catalysts

The specific surface area (SSA) of the support and Cu/CZ catalysts was determined using the BET method (Brunauer-Emmet-Teller) by N<sub>2</sub> adsorption at 77.35 K on the ASAP 2010 apparatus. Before measurements, the samples were degassed at 378 K until a stable vacuum of ca. 10<sup>-3</sup> Pa was reached.

The XRD patterns were recorded on a Siemens D5005 (Bruker-AXS, Germany) apparatus using CuK<sub>α</sub> radiation and operating at 30 kV and 50 mA. The data were collected in the 2θ range of 10°–90°.

Scanning electron microscopy (SEM) analysis was performed using SEM QUANTA 250 FEG (FEI, USA) microscope equipped with EDS detector (type SDD Apollo 10, EDAX) with resolution 129.11 eV. The measurements of surface morphology and images of the samples were carried out in high vacuum, under the acceleration voltage equal to 10 kV using LFD (SED/BSED) detector. The chemical composition of the examined samples was established by using EDS detector under the acceleration voltage 30 kV; quantitative and qualitative analysis—under high vacuum, elemental mapping—under low vacuum. The quantitative measurements

**Table 1** BET and structural properties of Cu/CZ catalyst and the support

| Catalyst  | SSA (m <sup>2</sup> /g) | Pore volume (cm <sup>3</sup> /g) | Crystallite size CZ (nm) | Crystallite size CuO (nm) | Lattice of CZ a (Å) | Composition (wt. %) SEM/EDX |           |           |           |
|-----------|-------------------------|----------------------------------|--------------------------|---------------------------|---------------------|-----------------------------|-----------|-----------|-----------|
|           |                         |                                  |                          |                           |                     | Cu                          | Ce        | Zr        | O         |
| CuO       | 29 ± 1                  | –                                | –                        | –                         | –                   | –                           | –         | –         | –         |
| CZ        | 138 ± 1                 | 0.32(2) <sup>a</sup>             | 7.9(8)                   | –                         | 5.32                | 0.00                        | 58.02(15) | 23.76(78) | 18.22(25) |
| Cu(2)/CZ  | 113 ± 1                 | 0.26(6)                          | 7.8(9)                   | –                         | 5.30                | 2.46(56)                    | 55.83(89) | 23.66(71) | 18.05(25) |
| Cu(4)/CZ  | 109 ± 1                 | 0.25(5)                          | 7.9(8)                   | –                         | 5.30                | 4.23(24)                    | 53.85(86) | 22.23(24) | 19.69(71) |
| Cu(10)/CZ | 101 ± 1                 | 0.23(3)                          | 7.9(8)                   | 56.8(6)                   | 5.30                | 10.82(89)                   | 46.86(87) | 20.09(10) | 22.23(36) |

<sup>a</sup> Numbers in brackets are 2σ errors of the last significant digits

were performed for 10 points. The arithmetic mean of the values and the standard deviations for all component elements of the samples were calculated.

Raman spectra were recorded on the Renishaw inVia spectrometer coupled with a Leica DM 2500 M microscope. The ion-argon laser beam operating with an excitation wavelength of 514 nm and the maximal laser power of 17 mW was used. The measurement parameters were as follows: laser power—10 % (1.7 mW), exposure time—10 s, number of scans—10, acquisition range 150–1500  $\text{cm}^{-1}$ . Raman point by point mapping with a step size of 20  $\mu\text{m}$  in both x and y directions was performed in the area of 80  $\mu\text{m} \times 80 \mu\text{m}$ . For each sample, 16 points were analyzed to obtain an insight into the sample structural heterogeneity.

### Catalytic test reaction

The oxidation–reduction and acid properties of the examined catalysts were determined using the conversion of isopropyl and *t*-butyl alcohol. The measurements were performed in a glass flow reactor with a fixed catalyst bed. The inner diameter of the reactor was 18 mm. Isopropyl or *t*-butyl alcohol was diluted with nitrogen. The mole fraction of both alcohols in nitrogen was 0.0179. The flow rate of the mixture was 20  $\text{dm}^3/\text{h}$ . The GHSV was 10,000  $\text{h}^{-1}$  in all measurements. The temperature was measured inside the catalyst bed. In each experiment, approximately 2 g of the sample was used. The measurements were performed in the kinetic region of the reaction (conversion below 20 %). In order to preserve steady state conditions of the experiments, after each increase of temperature, several samples of the product mixture were analyzed. The main measurements were performed when there was no further increase in the concentration of the products. The products were analyzed in situ using the gas chromatograph (Agilent 7890A) with a flame ionization detector (FID). The products of the reactions were separated using the capillary column type: DB FFAP with the diameter 0.32 mm and the length 60 m, the thickness of the film was 0.25  $\mu\text{m}$ . Before the reaction, all catalysts were standardized in the reactor at 400 K for 1 h in the nitrogen flow.

The experimental data were used to determine the selectivities, the apparent activation energies and the rates of reactions. The results are presented in the form of Arrhenius plots of  $\log(r)$  versus  $1/T$  [30]. This simplification is justified by the fact that the rate constant is directly proportional to the rate in this case. The linear character of all Arrhenius plots is preserved in the examined temperature range. The form of the rate equation of isopropyl alcohol conversion was elaborated previously [31] and is as follows:  $r = k \cdot p_{\text{alc}}^n$ , where  $r$  is the reaction rate,  $k$  is the rate constant,  $p_{\text{alc}}$  is the partial pressure of isopropyl alcohol  $n$  is the reaction order.

The rates of the reactions are calculated per unit surface area of catalysts and per number of  $\text{Cu}^{2+}$  active sites. The number  $n$  of  $\text{Cu}^{2+}$  active sites per unit mass of the catalyst was calculated from the equation:

$$n = \frac{2 \cdot S_{\text{CuO/CZ}}}{S_m}$$

where  $S_m$  is the mean surface area of the face in the unit cell in  $m^2$ ,  $S_{CuO/CZ}$  is the surface of CuO phase in the catalysts in  $m^2/g$ , 2 is the average number of  $Cu^{2+}$  cations on the face of the unit cell.

$S_{CuO/CZ}$  was calculated by multiplying SSA of the catalyst and the fraction of surface of the support occupied by CuO.  $S_m$  was calculated from the following equation:

$$S_m = \frac{\sum_i U_i \cdot P_i}{\sum_i U_i}$$

where  $P_i$  is the surface of the face  $i$  in  $m^2$ ,  $U_i$  is the contribution of the face  $i$  in the unit cell.

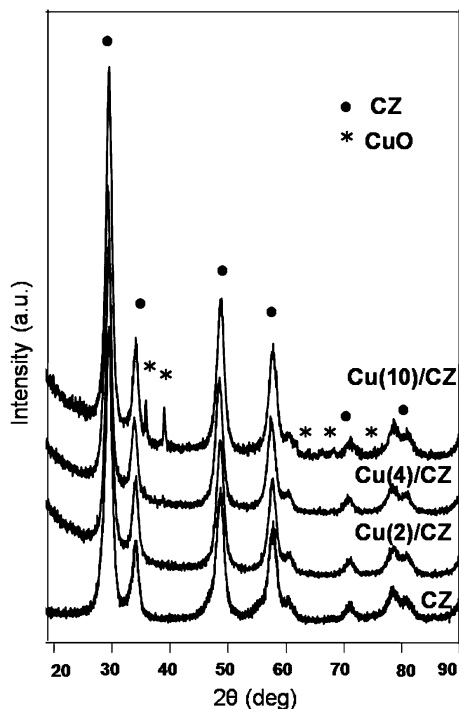
The calculations of  $P$  and  $U$  were performed for the faces with low Miller indices assuming that the faces (and their contributions) are proportional to the period in the direction perpendicular to the given face. The parameters of CuO unit cell taken into account in the calculations were those of tenorite structure:  $a = 4.6837 \text{ \AA}$ ,  $b = 3.4226 \text{ \AA}$ ,  $c = 5.1288 \text{ \AA}$ ,  $\beta = 99.54^\circ$ .

## Results and discussion

### X-ray diffraction

Fig. 1 presents XRD diffractograms of the support and Cu/CZ catalysts. The XRD diffractograms of the unmodified support and Cu/CZ catalysts show reflections typical for the fluorite cubic structure of the ceria-zirconia (JCPDS 01-078-0694). The detailed interpretation of the ceria-zirconia solid-solution XRD spectrum was presented in our previous work [25]. The XRD diffractogram of Cu(10)/CZ shows reflections characteristic for CuO tenorite structure (JCPDS 04-009-2287). These reflections are only observed for the catalyst with the highest Cu loading. For catalysts with 2 and 4 wt% of Cu, there were no reflections characteristic of the CuO phase. It suggests that in the catalysts Cu(2)/CZ and Cu(4)/CZ, the particles of copper oxide may be either amorphous or too small to be detected. Additionally, a certain amount of CuO may be partially integrated into  $CeO_2$  of the support. It is manifested by the decrease of lattice parameters of the support, because the ionic radius of  $Cu^{2+}$  ( $r_{Cu^{2+}} = 0.73 \text{ \AA}$ ) is smaller than the ionic radius of  $Ce^{4+}$  ( $r_{Ce^{4+}} = 0.97 \text{ \AA}$ ). [32–35]. The analysis of the values of lattice parameters collected in Table 1 shows the decrease of lattice parameters for all catalyst related to unmodified support. On the basis of these results, we can conclude that the CuO phase of Cu/CZ catalysts can be either amorphous (for lower loading) or crystalline with different crystallite size and different dispersion or can be partially incorporated in the ceria-zirconia surface–subsurface layers. The average size of crystallites of the CuO active phase and the CZ support calculated from the Scherrer equation is presented in Table 1. The values of crystallites size for pure and modified CZ support are the same. It indicates that during Cu/CZ preparation there is no sintering or augmentation of crystallites size of ceria zirconia mixed oxides.

**Fig. 1** XRD patterns of the support CZ (a) and catalysts: Cu(2)/CZ (b), Cu(4)/CZ (c), Cu(10)/CZ (d)



The crystallite size of CuO in Cu(10)/CZ is almost 8 times higher than for the CZ support and is equal to 56.8 nm, which suggests the agglomeration effect of CuO in this sample. For the catalysts with lower loading, the size of CuO crystallites was probably much lower than in Cu(10)/CZ, and presumably even lower than in the CZ support.

### Specific surface area and scanning electron microscopy

The values of specific surface area and pore volume for unmodified CZ, Cu/CZ samples and pure CuO are collected in Table 1. The specific surface area (SSA) of unmodified CZ is  $138 \text{ m}^2\text{g}^{-1}$ . After impregnation, the value of SSA decreases with the increase of CuO loading. The values of SSA for catalysts Cu(2)/CZ, Cu(4)/CZ and Cu(10)/CZ are: 113, 109 and  $101 \text{ m}^2\text{g}^{-1}$ . The drop of SSA for Cu(10)/CZ is significant. This effect confirms the existence of less dispersed and bigger agglomerates of CuO on the surface of the support. For Cu(2)/CZ and Cu(4)/CZ the SSA values are higher than for Cu(10)/CZ, which suggests better dispersion and lower crystallite size of the CuO active phase. Pore volumes of Cu(2)/CZ, Cu(4)/CZ, Cu(10)/CZ samples are practically identical. Additionally, it is also visible that in comparison with unmodified CZ support, the pore volumes of the Cu/CZ systems decrease. This effect is similar for all Cu/CZ samples irrespective of the amount of CuO. In all catalysts, during impregnation, smaller grains of CuO block pores of the CZ support.

In order to confirm information about the structure and dispersion of the CuO active phase on the surface of the CZ support, SEM/EDX analysis with elemental mapping was performed. SEM images of all catalysts reveal that the size of grains of the support is between 5 and 50  $\mu\text{m}$  and the shape of bigger grains is spherical. It is clearly seen that these surfaces are more exposed for the deposition of CuO, than the smaller grains of the support. Fig. 2 shows SEM mapping images of Cu(2)/CZ, Cu(4)/CZ, Cu(10)/CZ. For better visualization of the dispersion of copper oxide on the surface of ceria-zirconia mixed oxide, light color represents CuO and the support is depicted in dark color. The SEM images mapping of Cu/CZ catalysts show that better dispersion of CuO crystal phase is characteristic for samples with lower loading of Cu i.e.: Cu(2)/CZ, Cu(4)/CZ (Figs. 2a and b). When the amount of Cu is 10 wt % we can observe the formation of CuO agglomerates (marked with arrows) on the surface of the support (Fig. 2c).

### Raman spectroscopy

The XRD and SEM analysis of composition of Cu/CZ catalysts is well complemented by Raman spectroscopy. For all catalysts, Raman point by point mapping was performed to prove the existence of all phases on the surface of Cu(2)/CZ, Cu(4)/CZ, Cu(10)/CZ samples. From 16 spectra registered for each sample, two or three representative were chosen.

In the spectrum of pure CZ support three peaks are observed. According to the literature, the most intensive peak around  $475\text{ cm}^{-1}$  corresponds to a cubic fluorite structure [36]. The presence of weak bands at ca.  $302, 624\text{ cm}^{-1}$  is assigned to a tetragonal displacement of oxygen atoms from their ideal fluorite lattice positions [37]. In the crystalline pure CuO sample, three Raman bands centered at ca.  $297, 345$  and  $627\text{ cm}^{-1}$  are observed [38]. Fig. 3 shows three sets of spectra of Cu/CZ catalysts. Spectrum a corresponds to the component copper oxide phase of the Cu(10)/CZ catalyst. Spectrum b proves the presence of a mixture of CuO (bands centered at  $297, 344$  and  $627\text{ cm}^{-1}$ ) and CZ phase (band centered at  $475\text{ cm}^{-1}$ ). Spectrum c may be attributed to the CZ support with the most intensive band at  $475\text{ cm}^{-1}$ . Two residual peaks at  $295$  and  $625\text{ cm}^{-1}$  can be assigned to the CuO additive. There is no evidence of pure support on the surface of Cu(10)/CZ catalyst. It indicates that in this catalyst, the significant coverage of the support with the active phase is achieved. Additionally, in some areas agglomerates of copper oxide are present (pure phase of CuO was also registered). Spectra d, e and f correspond to the CuO component phase (bands centered at  $297, 343$  and  $630\text{ cm}^{-1}$ ), Cu/CZ mixture phase (bands centered at  $297, 345, 474\text{ cm}^{-1}$ , and  $629\text{ cm}^{-1}$ ) and CZ (bands centered at  $302, 475$  and  $625\text{ cm}^{-1}$ ) phase of Cu(4)/CZ catalyst. Contrary to the sample Cu(10)/CZ, the Raman spectra of Cu(4)/CZ show the presence of the pure CZ phase. The smaller amount of CuO deposited on the surface of the support entails uncovered areas of the CZ phase. The spectra of Cu/CZ mixture (bands centered at  $297, 344, 475$  and  $627\text{ cm}^{-1}$ , Fig. 3f) and CZ support (bands centered at  $302, 475$  and  $624\text{ cm}^{-1}$ , Fig. 3g) were registered for sample Cu(2)/CZ. There is no trace of CuO pure phase in this catalyst. It may be due to the homogenous dispersion of copper oxide on the surface of ceria-zirconia and the lack of agglomeration effect





**Fig. 2** SEM mapping images of Cu(2)/CZ (a), Cu(4)/CZ (b), Cu(10)/CZ (c)

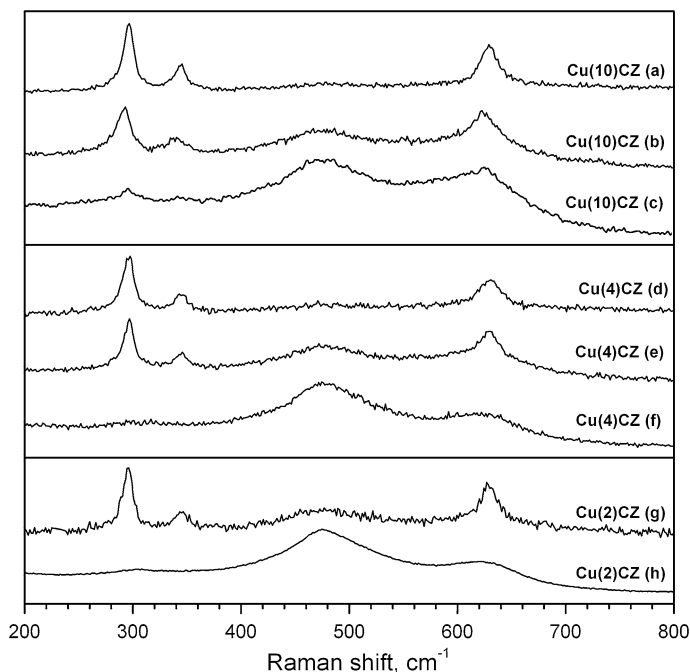


**Fig. 3** Raman spectra of samples: Cu(10)/CZ (a–c), Cu(4)/CZ (d–f), Cu(2)/CZ (g, h)

confirmed by SEM images mapping. The values of Raman shifts for CuO component phase in all Cu/CZ catalysts are similar to those of pure copper oxide. It may indicate that on the surface of the catalysts the bigger grains of CuO are more exposed.

### Kinetic measurements of isopropyl alcohol conversion

The conversion of isopropyl alcohol may lead to three main products: acetone, propene and diisopropyl ether. Acetone is produced over redox and/or base surface active sites, whereas propene and diisopropyl ether are formed over acid–base active centers of oxide catalysts [8, 15, 16, 39]. In the case of oxides with one stable oxidation state, the dehydrogenation proceeds over basic Lewis active sites. For metal oxides in various oxidation states (e.g.: Ce<sup>4+</sup> and Cu<sup>2+</sup> ions), the dehydration and dehydrogenation take place over redox active sites, because according to the literature, redox sites (metal cations M<sup>n+</sup>) reveal both redox properties and Lewis type acidity at higher temperature [8, 15].

The results of kinetic measurements of dehydrogenation of isopropyl alcohol to acetone over Cu/CZ catalysts, pure CuO and unmodified CZ support are displayed in Fig. 4 in the form of Arrhenius plots (the reaction rate is calculated with respect to the unit surface area of the catalyst). Dehydrogenation to acetone starts in the lower temperature range for Cu/CZ than for pure CuO and CZ support. All Cu/CZ

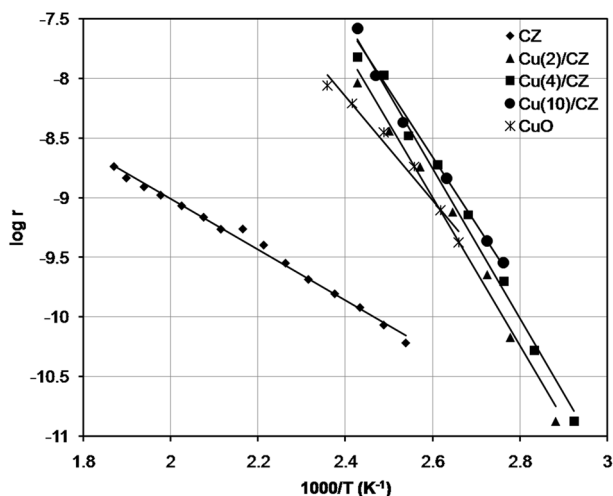


**Fig. 4** Arrhenius plots for the dehydrogenation of isopropyl alcohol to acetone over catalysts: Cu(2)/CZ, Cu(4)/CZ, Cu(10)/CZ, CZ and CuO, the reaction rate in mol/(s m<sup>2</sup>)

catalysts are more active than the unmodified support and reveal similar activity to the pure copper oxide. It indicates that for Cu/CZ, dehydrogenation runs over active sites situated on the active phase (deposited CuO) of the catalyst. It also shows the promotional effect of the support, because contrary to the pure CuO, in Cu/CZ catalysts, only a fraction of the surface is active in dehydrogenation, whereas the reaction rate is calculated with respect to the entire specific surface area of the catalyst.

The activity of Cu/CZ is hardly susceptible for the changes in the amount of deposited CuO. It is only slightly higher after increasing the amount of copper oxide. Two major aspects are crucial in understanding of such behavior. The first one is the number of active sites. On one hand, deposition of the higher amount of the active phase should create more active sites. On the other hand, the agglomeration effect occurs (confirmed by SEM images mapping analysis and XRD). As a result, the higher amount of deposited copper oxide causes only the growth of bigger crystallites and does not create additional active sites. The second aspect is the influence of the support on the active phase of the catalyst. The higher the dispersion of the CuO phase (smaller size of crystallites) on the surface of CZ support, the better the interaction between copper oxide and CZ. Active sites located on bigger crystallites may act like these of pure CuO, because they are isolated from the support.

Better visualization of the influence of the effects discussed above is achieved when comparing the activity of the examined catalysts by taking into account the reaction rate calculated with respect to the amount of Cu<sup>2+</sup> active sites (Fig. 5). All Cu/CZ catalysts are more active than pure CuO. The increase in activity of supported samples confirms the promotional effect of ceria zirconia mixed oxides on the activity of the CuO phase. The features of the CZ support such as easy

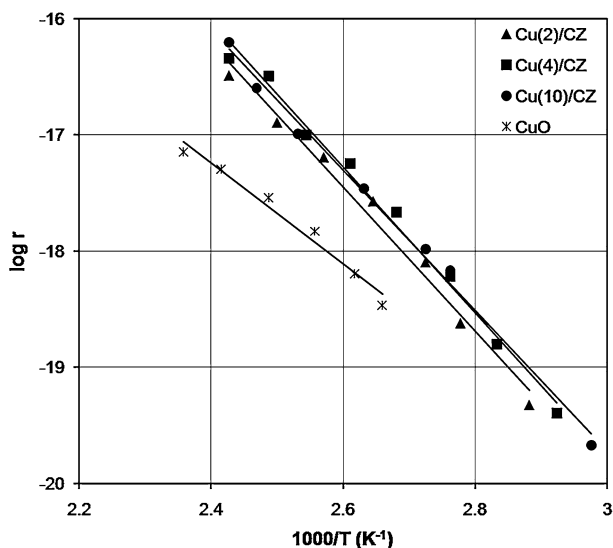


**Fig. 5** Arrhenius plots for the dehydrogenation of isopropyl alcohol to acetone over catalysts: Cu(2)/CZ, Cu(4)/CZ, Cu(10)/CZ, CuO, the reaction rate in mol/(s  $n_{Cu}^{2+}$ ),  $n$ -the number of  $Cu^{2+}$  active sites

change of oxidation state of ceria from  $Ce^{4+}$  to  $Ce^{3+}$  and extraordinary mobility of lattice oxygen/oxygen vacancies from the bulk to the surface, induce promotional effect on the redox properties of the active phase/CZ support catalytic systems [19, 20, 24, 25]. It has been found in the literature that there is a very strong interaction between Cu and Ce atoms. When the reduction of  $Cu^{2+}$  to  $Cu^+$  or  $Cu^0$  occurs, the  $Ce^{4+}$  ions from the support act as oxidizing agents for  $Cu^{2+}/Cu^+$  particles ( $Cu^+ + Ce^{4+} = Ce^{3+} + Cu^{2+}$ ). The equilibrium between copper and ceria cations is achieved and it stabilizes copper cations on the surface of the support, even in strongly reducing atmosphere [34, 39]. In Cu/CZ catalysts, the interaction between the active phase and the support is strong enough to induce the most effective regeneration of the active phase surface, which leads to the rise in the reaction rate while increasing the temperature. This is confirmed by the values of activation energy of dehydrogenation to acetone (Table 2). The values of activation energies for all Cu/CZ catalysts are much higher than for pure CuO. It shows the influence of the CZ support on the catalytic activity of deposited CuO. The value of activation energy is very sensitive to changes in the number of active sites of the catalyst [15].

**Table 2** Activation energy of isopropyl alcohol conversion to acetone

| Catalyst  | $E_a$ (kJ/mol) Dehydrogenation to acetone |
|-----------|---|
| CZ        | $40.7 \pm 1.0$                            |
| Cu(2)/CZ  | $118.4 \pm 6.3$                           |
| Cu(4)/CZ  | $125.0 \pm 4.4$                           |
| Cu(10)/CZ | $107.8 \pm 4.8$                           |
| CuO       | $83.3 \pm 6.7$                            |

**Table 3** Selectivity of isopropyl alcohol conversion to acetone and propene

| Catalyst  | Selectivity (%) |         |         |         |
|-----------|-----------------|---------|---------|---------|
|           | 390 K           |         | 410 K   |         |
|           | Propene         | Acetone | Propene | Acetone |
| CZ        | 0.1             | 99.9    | 0.3     | 99.7    |
| Cu(2)/CZ  | 0.3             | 99.7    | 0.1     | 99.9    |
| Cu(4)/CZ  | 0.2             | 99.8    | 0.2     | 99.8    |
| Cu(10)/CZ | 0.1             | 99.9    | 0.3     | 99.7    |
| CuO       | 0.2             | 99.8    | 0.1     | 99.9    |

When the reaction runs over active sites, which are deactivated during the process, the value of activation energy decreases. When the creation of new active sites occurs during the process the activation energy increases. If the number of active sites remains the same, the value of activation energy depends mainly on the properties of active sites. In Cu/CZ catalysts, where the type of the active phase is the same for all samples, the differences in activation energy values are due to the efficient interaction between the active phase and the support. Higher values of activation energy for Cu/CZ samples than for pure CZ support indicate that the obtained catalysts exhibit better redox properties. It is also confirmed by the measurement of temperature programmed reduction of the catalysts by hydrogen ( $H_2$ -TPR) shown in our previous work [25]. The consumption of  $H_2$  is higher for Cu/CZ catalysts than for the CZ support. The reduction is shifted to the lower temperature range. It shows that Cu/CZ catalysts are more susceptible for reduction than the pure support.

The values of selectivity of isopropyl alcohol conversion are collected in Table 3. All examined catalysts, pure CuO and unmodified support are active mainly in the dehydrogenation to acetone. Only traces of dehydration products (propene, diisopropyl ether) are detected. The low activity in dehydration is due to the weak acid properties of Lewis active sites of the catalysts. These sites are activated at higher temperatures, which is clear from the data obtained for the pure support. Because of the lower activity of CZ, the kinetic measurements were performed at higher temperatures than for Cu/CZ samples. For pure CZ, the rates of conversion to propene and to acetone become equal at the temperature ca. 515 K. For Cu/CZ catalysts, the kinetic measurements were performed at lower temperatures (340–410 K) because of their higher activity. Under these conditions, Lewis acid sites are barely active. The creation of diisopropyl ether is only observed for the pure support at temperatures above 480 K.

### Kinetic measurements of *t*-butyl alcohol conversion

*t*-Butyl alcohol conversion was carried out to confirm acid and redox properties of the active phase in Cu/CZ catalysts. The molecule of *t*-butyl alcohol is bigger than the molecule of isopropyl alcohol. The size of the *t*-butyl alcohol molecule limits penetration into the CZ support in Cu/CZ samples. In this case, the direct reaction

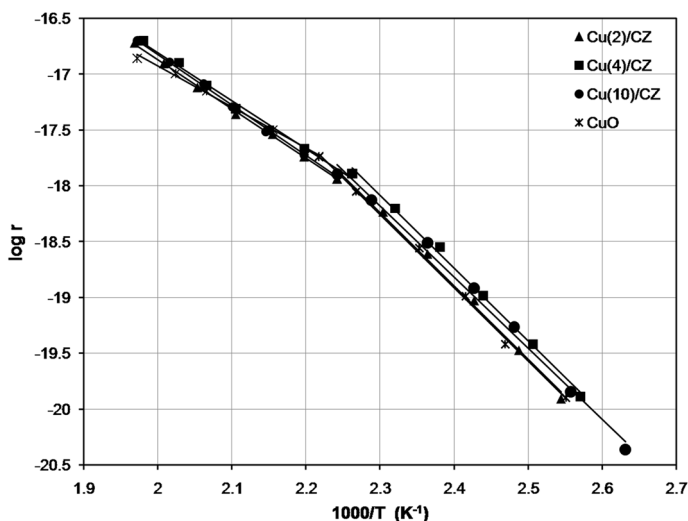


**Fig. 6** Arrhenius plots for the dehydrogenation of *t*-butyl alcohol to isobutene over catalysts: Cu(2)/CZ, Cu(4)/CZ, Cu(10)/CZ, CuO, the reaction rate in mol/(s nCu<sup>2+</sup>), where n—the number of Cu<sup>2+</sup> active sites

over active sites of the support is no longer possible. Therefore, *t*-butyl alcohol conversion is convenient to probe the activity of CuO phase in Cu/CZ systems. This assumption is well demonstrated by the results of kinetic measurements of dehydration of *t*-butyl alcohol to isobutene over Cu/CZ catalysts and pure CuO (Fig. 6) (the reaction rate is calculated per number of Cu<sup>2+</sup> active sites). The activities of Cu(2)/CZ, Cu(4)/CZ, Cu(10)/CZ in the higher and lower range of temperature are practically the same and overlap the activity of pure CuO. These data prove similar properties of acid active centers of pure CuO and Cu/CZ samples.

The results of the kinetic measurements of dehydration of *t*-butyl alcohol to isobutene over Cu/CZ catalysts, CuO and the support are shown in Fig. 7. The reaction rate is calculated per unit surface area of the catalyst, which enables the discussion about the number of sites on the surface of Cu/CZ being active in the examined reaction. Cu/CZ catalysts and pure copper oxide show higher activity than the support. Copper oxide exhibits the best acid properties. Therefore, the number of acid active sites of Cu/CZ catalysts should increase with higher loading of CuO. This tendency is maintained only at higher temperatures (above 450 K) for Cu/CZ catalysts. At lower temperatures, the activity increases with higher loading of the active phase, but only for Cu(2)/CZ and Cu(4)/CZ samples, whereas the activity of Cu(10)/CZ is similar to the activity of Cu(4)/CZ. This phenomenon can be associated with the availability of the active sites on the surface of the catalysts studied. The active sites of catalysts with low loading are more accessible than in Cu(10)/CZ. The size of crystallites of the active phase and the degree of dispersion play an important role. For the catalysts with low loading, the active phase is well dispersed on the surface of the support, which leads to the increase in the number of active sites and the higher catalytic activity. Therefore, for 2 and 4 wt% CuO

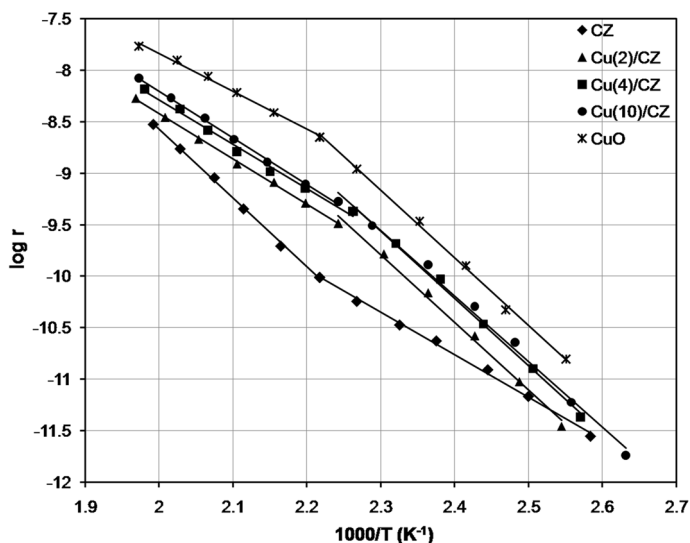


**Fig. 7** Arrhenius plots for the dehydrogenation of *t*-butyl alcohol to isobutene over catalysts: Cu(2)/CZ, Cu(4)/CZ, Cu(10)/CZ, CZ and CuO, the reaction rate in mol/(s m<sup>2</sup>)

**Table 4** Activation energy of *t*-butyl alcohol conversion to isobutene and acetone

| Catalyst  | E <sub>a</sub> (kJ/mol)                   |   |                               |
|-----------|---|---|-------------------------------|
|           | Dehydration to isobutene<br>(below 450 K) | Dehydration to isobutene<br>(above 450 K) | Dehydrogenation<br>to acetone |
| CZ        | 78.8 ± 1.9                                | 122.7 ± 3.5                               | 89.9 ± 3.2                    |
| Cu(2)/CZ  | 120.3 ± 4.9                               | 84.3 ± 1.7                                | 60.4 ± 6.3                    |
| Cu(4)/CZ  | 116.7 ± 5.4                               | 87.6 ± 3.2                                | 81.6 ± 3.4                    |
| Cu(10)/CZ | 117.4 ± 4.5                               | 88.5 ± 1.6                                | 71.6 ± 5.2                    |
| CuO       | 125.3 ± 4.0                               | 70.5 ± 3.3                                | 69.3 ± 4.7                    |

loading, the catalytic activity increases. In the case of Cu(10)/CZ catalyst, the significant amount of active phase exists in the form of agglomerates, so the access to acid sites is difficult. As a result, no significant increase in activity is observed for the highest loading in comparison to other Cu/CZ catalysts. The available literature data suggest that Ce<sup>4+</sup>/Ce<sup>3+</sup>, Zr<sup>4+</sup> ions of the support are acid sites [40]. However, in the case of Cu/CZ catalysts, mainly CuO molecules act as acid sites. This is confirmed by the values of activation energy of the catalysts studied, which are similar to the value of CuO rather than CZ (Table 4). Since the molecule of *t*-butyl alcohol is large, its access to Ce<sup>4+</sup>/Ce<sup>3+</sup>, Zr<sup>4+</sup> ions can be difficult, when CuO is deposited on the support. The accessibility of these ions and their direct participation in the conversion of *t*-butyl alcohol can be limited by higher loading and better dispersion of the active phase on the surface of the support. At higher

**Table 5** Selectivity of *t*-butyl alcohol conversion to isobutene and acetone

| Catalyst  | Selectivity (%) |         |           |         |           |         |
|-----------|-----------------|---------|-----------|---------|-----------|---------|
|           | 400 K           |         | 420 K     |         | 440 K     |         |
|           | Isobutene       | Acetone | Isobutene | Acetone | Isobutene | Acetone |
| CZ        | 67.4            | 32.6    | 85.3      | 14.7    | 93.6      | 6.4     |
| Cu(2)/CZ  | 40.0            | 60.0    | 67.0      | 33.0    | 84.6      | 15.4    |
| Cu(4)/CZ  | 48.9            | 51.1    | 74.6      | 25.4    | 89.0      | 11.0    |
| Cu(10)/CZ | 40.5            | 59.5    | 67.5      | 32.5    | 85.1      | 14.9    |
| CuO       | 52.0            | 48.0    | 63.6      | 36.4    | 72.9      | 27.1    |

temperatures, differences in activity between Cu(4)/CZ and Cu(10)/CZ catalysts are more noticeable. The activity increases with higher loading of the active phase, but above 450 K, the increase of the reaction rate is lower than below this temperature (the slope of plots decreases). It is due to the fact that at higher temperatures Cu<sup>2+</sup> ions are reduced to Cu<sup>+</sup> and further to Cu<sup>0</sup>, which induces a decrease in the number of acid active sites [41]. It is consistent with H<sub>2</sub>-TPR results reported in [25], where in the similar temperature range, reduction of CuO and CeO<sub>2</sub> on the surface was observed. The reduction of Cu<sup>2+</sup> also causes the decrease in the activation energy (Table 4).

Table 5 shows selectivity of *t*-butyl alcohol conversion. Apart from isobutene, the formation of acetone is also observed. Acetone is probably formed as a result of destructive oxidation of *t*-butyl alcohol. The oxidizing agent is the lattice oxygen of CuO and/or the support (measurements were performed in the absence of gaseous oxygen). The other possibility is that *t*-butyl carbocation undergoes oxidation, before transformation to isobutene [13]. All Cu/CZ catalysts, as well as the support and pure CuO exhibit activity in the formation of acetone. The results of the kinetic measurements of acetone formation over Cu/CZ catalysts, CuO and the support are shown in Fig. 8 (the rate of reaction was calculated with respect to the unit surface area of the catalyst). The support is the least active in the formation of acetone. Although it can release the lattice oxygen, it contains weaker active sites over which the formation of acetone can proceed. CuO exhibits the highest activity in the formation of acetone. It undergoes gradual reduction during the reaction. At around 430 K a rapid increase in activity is observed, which can be explained by the reduction of surface layers of CuO. Reduction of CuO to Cu is a topochemical process accompanied by generation of dislocations and other extended defects in whose vicinity low-coordinated Cu atoms with enhanced catalytic activity can be located [42, 43]. Cu/CZ catalysts exhibit lower activity than pure CuO, but are more active than the pure support. Among Cu/CZ catalysts Cu(2)/CZ is slightly less active than Cu(4)/CZ and Cu(10)/CZ. Cu(4)/CZ is more active than Cu(2)/CZ which is caused by the higher number of active redox sites participating in the reaction. Despite higher loading with the active phase, the activity of Cu(10)/CZ is similar to other catalysts, which is due to the size and dispersion of CuO crystallites. The agglomeration effect hinders surface re-oxidation and lowers the number of active



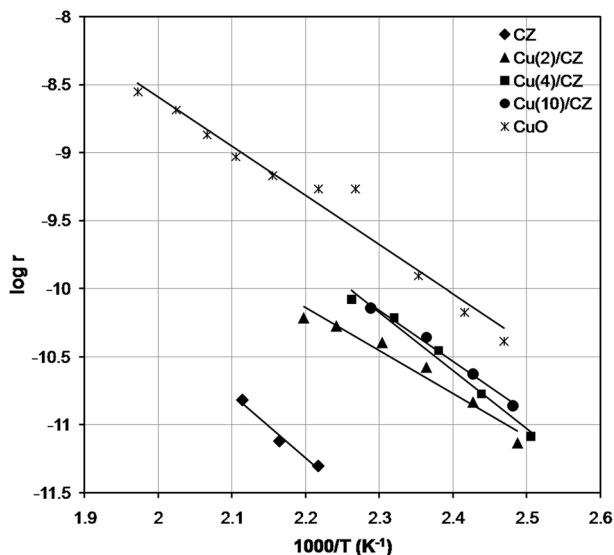


**Fig. 8** Arrhenius plots for the oxidation of *t*-butyl alcohol to acetone over catalysts: Cu(2)/CZ, Cu(4)/CZ, Cu(10)/CZ, CZ and CuO, the reaction rate in mol/(s m<sup>2</sup>)

sites. Cu/CZ catalysts do not show the rapid increase in activity at 430 K, as in the case of pure CuO (Fig. 8). Above 430 K, the activity of Cu/CZ catalysts starts to decrease, which is caused by the insufficient amount of lattice oxygen in the active phase to maintain the reaction.

## Conclusions

A series of catalysts Cu/CZ with various amounts of CuO active phase was synthesized. The composition, morphology, redox and acid properties of the obtained samples were established. Raman spectroscopy, XRD and SEM-mapping analysis confirmed good dispersion of the active phase for less loaded catalysts. The agglomeration effect was observed for the catalyst with the highest amount of CuO. The conversion of isopropyl alcohol showed that all Cu/CZ catalysts revealed major activity in dehydrogenation of alcohol to acetone. It indicated that the reaction mainly ran over redox active centers. Conversion of *t*-butyl alcohol confirmed the presence of acid centers. It has been found that the increase in activity of Cu/CZ catalysts compared with unmodified CZ support is caused by the CuO active phase. Additionally, it has been shown that catalytic properties of Cu/CZ samples depend on the dispersion of the active phase on the surface of the support. Good dispersion implies both better accessibility of redox and acid sites and efficient interaction between CuO and ceria zirconia mixed oxides. This interaction improves redox properties and stabilizes the acidity of the surface.

## References

1. Thomas JH, Thomas WJ (2008) Principles and practice of heterogeneous catalysis, chap. 1. Wiley-VCH, Weinheim
2. Abello MC, Gomez MF, Ferretti O (2001) *Appl Catal A* 207:421–431
3. Haffad D, Chambellan A, Lavelly JC (2001) *J Catal A* 168:153–164
4. Cutrufello MG, Ferino I, Monaci R, Rombi E, Solinas V (2002) *Top Catal* 19:225–240
5. Busca G, Finocchio E, Ramis G, Ricchiardi G (1996) *Catal Today* 32:133–143
6. Davydov A (2003) *Molecular spectroscopy of oxide catalyst surface*. Wiley, London
7. Hadjiivanov KI (2000) *Catal Rev Sci Eng* 42:71–144
8. Turek W, Haber J, Krowiak A (2005) *Appl Surf Sci* 252:823–827
9. Schlunt P, Chau PC (1986) *J Catal* 102:348–356
10. Haag WO, Pines H (1960) *J Am Chem Soc* 82:387–391
11. Roosmalen AJ, Hartmarin MCG, Mol JC (1980) *J Catal* 66:112–120
12. Suzuki I (1981) *J Catal* 68:220–222
13. Turek W, Strzeżek J, Krowiak A (2012) *Reac Kinet Mech Cat* 107:115–125
14. Turek W, Lapkowski M, Debiec J, Krowiak A (2005) *Appl Surf Sci* 252:847–852
15. Turek W, Krowiak A (2012) *Appl Catal A* 417:102–110
16. Ortiz-Islas E, Lopez T, Navarrete J, Bokhimi X, Gómez R (1998) *J Sol-Gel Sc Technol* 13:1043–1047
17. Adamowska M, Muller S, Da Costa P, Krzton A, Burg P (2007) *Appl Catal B* 74:278–289
18. Adamowska M, Krzton A, Najbar M, Camra J, Djega-Mariadassou G, Da Costa P (2009) *Appl Catal B* 90:535–544
19. Gómez-García MA, Pitchon V, Kiennemann A (2005) *Environ Int* 31:445–467
20. Damyanova S, Pawelec B, Arishtirova K, Martinez Huerta MV, Fierro JLG (2008) *Appl Catal A* 337:86–96
21. Agula B, Deng QF, Jia ML, Liu Y, Zhaorigetu B, Yuan ZY (2011) *Reac Kinet Mech Cat* 103:101–112
22. Xu S, Yan X, Wang X (2006) *Fuel* 85:2243–2247
23. Bruix A, Rodriguez JA, Ramirez PJ, Senanayake SD, Evans J, Park JB, Stacchiola D, Liu P, Hrbek J, Illas F (2012) *J Am Chem Soc* 134:8968–8974
24. Trovarelli A (1996) *Catal Rev Sci Eng* 38:439–520
25. Radlik M, Adamowska M, Łamacz A, Krztoń A, Da Costa P, Turek W (2013) *Reac Kinet Mech Cat* 109:43–56
26. Łamacz A, Krzton A, Djega-Mariadassou G (2011) *Catal Today* 176:126–130
27. Granger P, Parvulescu VI (2011) *Chem Rev* 111:3155–3207
28. Little LH (1966) *Infrared spectra of adsorbed species*. Academic Press, London
29. Trovarelli A, De Leitenburg C, Dolcetti G, Lorca JL (1995) *J Catal* 151:111–124
30. Chorkendorff I, Niemantsverdriet JW (2003) *Concepts of modern catalysis and kinetics*. Wiley-VCH, Weinheim, p 51
31. Haber J, Turek W, Wolna A (2003) *Ann Pol Chem Soc* 3:1229–1231
32. Dow WP, Wang YP, Huang TJ (2000) *Appl Catal A* 190:25–34
33. Sedmak G, Hocevar S, Levec J (2003) *J Catal* 213:135–150
34. Djinovic P, Levec J, Pintar A (2008) *Catal Today* 138:222–227
35. He Ch, Yu Y, Shen Q, Chen J, Qiao N (2014) *Appl Surf Sci* 297:59–69
36. Lianjun L, Zhijian Y, Bin L, Lin D (2010) *J Catal* 275:45–60
37. Letichevsky S, Tellez CA, de Avillez RR, da Silva MIP, Fraga MA, Appel LG (2005) *Appl Catal B* 58:203–210
38. Xu JF, Ji W, Shen ZX, Li WS, Tang SH, Ye XR, Jia DZ, Xin XQ (1999) *J Raman Spectrosc* 30:413–425
39. Hocevar S, Batista J, Levec J (1999) *J Catal* 184:39–48
40. Daturi M, Binet C, Lavalley JC, Galtayries A, Sporken R (1999) *Phys Chem Chem Phys* 1:5717–5724
41. Busca G (1998) *Catal Today* 41:191–206
42. Burbano M, Sian N, Marrocchelli D, Salanne M, Graeme WW (2014) *Phys Chem Chem Phys* 16:8320–8331
43. Liu P, Stacchiola D, Hrbek J, Rodriguez JA (2011) *J Am Chem Soc* 133:11474–11477